EXTENDED ABSTRACTS

VOLUME 81-1

Battery
Corrosion
Dielectrics and Insulation
Electronics
Electrothermics and Metallurgy
Energy Technology
Industrial Electrolytic
Organic and Biological Electrochemistry
Physical Electrochemistry
New Technology Subcommittee

* * * * * *

SPRING MEETING

MINNEAPOLIS, MINNESOTA

MAY 10-15, 1981

Note:

Presentation of a paper at a Technical Meeting of this Society does not guarantee publication in full by the Society. Extended Abstracts contained herein may not be reprinted and may not be digested by publications other than those of The Electrochemical Society in excess of 1/6 of the material presented.

* * * * * *

Not all illustrations to be presented during paper delivery are reproduced here. Production limitations of this volume caused illustration reduction to a point where a phenomenon described by the author may have, in some cases, been lost in reproduction. All magnifications are those existing before photographic reduction.

Printed in the United States of America

THE ELECTROCHEMICAL SOCIETY, INC.
Spring Meeting, Minneapolis, Minnesota
May 10-15, 1981

Extended Abstracts
of
BATTERY DIVISION/ENERGY TECHNOLOGY GROUP/
INDUSTRIAL ELECTROLYTIC DIVISION

Subject:
Porous Electrodes

The Electrochemical Society, Inc., 10 South Main St., Pennington, NJ 08534

CONTENTS

Abstract No. 1

DISTRIBUTION OF POTENTIAL IN LEAD-ACID BATTERY ELECTRODES

W. G. Sunu and B. W. Burrows
Gould Laboratories
40 Gould Center
Rolling Meadows, IL 60008

Optimization of lead-acid battery design to minimize the use of lead and to improve performance is becoming increasingly important. Grid geometry is a key variable that is amenable to optimization. In particular, the potential distribution over the surface of an electrode can be readily predicted from a model and the predictions can be checked experimentally. It was the aim of this work to compare model predictions with experimental data and to explore some implications of the model predictions.

Model: A mathematical model of a grid structure was developed using the approach described by Tiedemann et al (1). The grid is represented by a resistance network connecting nodes or points where grid members intersect. Kirchoff's first law was applied to each node and the resulting equations were solved using a matrix inversion technique. Uniform current density over the plate surface was assumed. Two diagonal grid members radiating from the current-collecting tab were included in the model. The model was used to predict potential distributions for a variety of grid configurations.

Experimental: Three-plate cells were used to measure the potential distribution over the face of automotive battery plates. The grids were 120 mm high and 142 mm wide. The positive and negative grids were 1.62 mm and 1.19 mm thick and weighed 64 g and 47 g, respectively. Two types of cells were used; one had a center positive and one a center negative. The middle electrode had Teflon®-coated gold wires attached to the grid at 42 different locations (6 vertical x 7 horizontal) for the direct measurement of grid potentials as a function of discharge rate, temperature, and plate width.

Results: The potential data were fitted to a two-dimensional equation:

$$V(x,y) = \sum_{n=o}^{3} \sum_{m=o}^{4} A_i x^m y^n \quad \text{where } i = 4m + n$$

where V is the grid potential in mV, the A's are polynomial coefficients (twenty in all) of vertical distance, y, and horizontal distance, x, respectively. The polynomial fit matched the data to within 0.5% and was used to produce iso-potential diagrams such as those shown in Fig. 1. In Fig. 2, the potential difference between the tab and the diagonally opposite corner is plotted as a function of discharge current and plate width for fully charged plates. Fig. 2a was obtained with full-size plates and Fig. 2b was obtained with plates of three different widths but with the same apparent current density of 293 mA cm^{-2}.

Some observations from this work are summarized below:

- Most of the potential loss occurs in the region near the current-collecting tab (see Fig. 1). Thus 50% of the total loss occurs over just 15% of the positive plate area and 9% of the negative plate area.
- The potential difference between a tab and the opposite corner of a plate was always 15% greater in the negative plate than in the positive plate despite the presence of the porous lead active material on the negative.
- The overall plate potential loss was linearly proportional to (a) the discharge current (see Fig. 2a) and to (b) the plate width when discharged with the same apparent current density (see Fig. 2b). The latter observation shows that decrease of the plate area can significantly decrease the cell polarization and improve the high rate performance on a battery if the total apparent plate area is kept constant.
- Grid resistance, R_g, increases linearly with temperature according to the equation:

$$R_g = R_{25} \left[1 + 0.00276\ (T-25)\right]$$

where R_{25} is the resistance in ohm measured at 25°C and T is the temperature in °C.

- During formation at 1A per plate the positive plate resistance was nearly independent of the state-of-charge with the tab-to-corner potential loss being 1.4 mV at the beginning and 1.5 mV at the end of formation. On the other hand, the loss in the case of the negative plate decreased from 2.3 mV at the start to 1.6 mV at the end indicating that one-third of the current in the negative is carried by the active material. This is in good agreement with data of Puzey and Orriel (2).

Discussion: The utility of the model will be illustrated by showing the effects of (a) location and number of tabs, (b) diagonal grid members, (c) tapered grid members and (d) grid geometry on potential distribution at positive and negative automotive battery plates.

References:

1. W. Tiedemann, J. Newman and F. DeSua, Power Sources 6, (D. Collins, ed.), p 15 (1976).

2. J. E. Puzey and W. M. Orriel, Power Sources 2, (D. Collins, ed.) p 121 (1968).

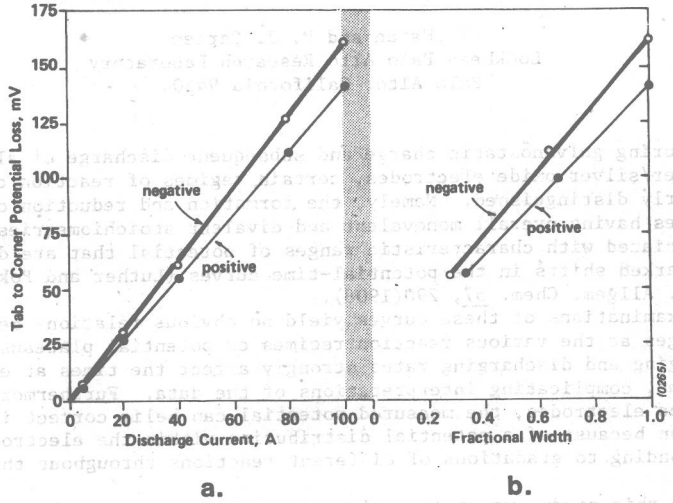

FIGURE 2

POTENTIAL LOSSES BETWEEN A TAB AND THE OPPOSITE CORNER OF SLI PLATES

a. Measured with standard size plates

b. Measured with same apparent current density of 293mA/cm^2

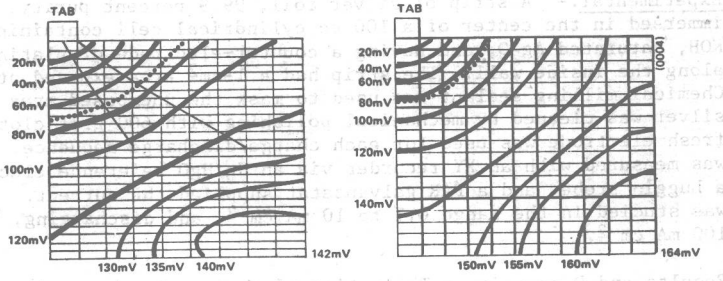

FIGURE 1

POTENTIAL DISTRIBUTION IN SLI PLATES MEASURED DURING DISCHARGE AT 100A PER PLATE (293mA/cm^2)

.... Isopotential curve corresponding to 50% of maximum potential loss

Abstract No. 2

RATIOS OF AgO/Ag_2O IN POROUS SILVER OXIDE ELECTRODES

T. Katan and P. J. Carlen
Lockheed Palo Alto Research Laboratory
Palo Alto, California 94304

During galvanostatic charge and subsequent discharge of alkaline silver/silver oxide electrodes, certain regimes of reaction can be clearly distinguished. Namely, the formation and reduction of silver oxides having overall monovalent and divalent stoichiometries are associated with characteristic ranges of potential that are discernable by marked shifts in the potential-time curves (Luther and Pokorny, Z. Anor. Allgem. Chem. 57, 290(1908).

Examinations of these curves yield no obvious relations between the charges at the various reaction regimes or potential plateaus. The charging and discharging rates strongly affect the times at each regime, complicating interpretations of the data. Furthermore, with porous electrodes, the measured potential can belie correct interpretation because of a potential distribution within the electrode, corresponding to gradations of different reactions throughout the porous mass.

In this study, we utilize planar rather than porous electrodes and determine the ratios of times (charges) at the various reaction regimes during charge and discharge. We maintain uniform current (potential) distribution. To better understand the complicating effects of rates on these ratios, we conduct galvanostatic studies both with varying charge rate for a given discharge rate, and with varying discharge rate for a given charge rate. Definite numerical ratios appear under these conditions that can be interpreted in terms of reaction mechanisms and porous electrode behavior.

Experimental.- A strip of silver foil, 99.9 percent purity, was immersed in the center of a 100 cc cylindrical cell containing 10 M KOH, saturated Ag_2O, and having a counter-electrode of platinum gauze along the inside wall. The strip had a 1-cm^2 area exposed at its tip. Chemical-milling sealant was used to mask the unexposed area after the silver was cleaned by mechanical polishing with 600 grit cloth. A fresh electrode was used for each charge/discharge sequence. Potential was measured with an XY recorder via an Hg/HgO reference electrode with a Luggin probe, and a PAR galvanostat supplied the current. Charging was studied in the range 0.1 to 10 mA cm^{-2}, and discharging, 0.3 to 100 mA cm^{-2}.

Results and Discussion.- The ratios of charges in the various reaction regimes that have been well characterized in the past were determined from the shapes of the potential-time curves. We designate the charges for the first and second reaction regime, usually attributed to Ag_2O and AgO formation, as Q_1 and Q_2, and for the third and fourth, usually attributed to AgO and Ag_2O reduction, as Q_3 and Q_4, respectively.

From plots of Q_1/Q_2, Q_2/Q_3, and Q_3/Q_4 versus the varied currents,

the ratios 1/3, 2/1, and 3/5, respectively, were found to be favored. Deviations from these ratios occurred at very high current densities, when excessive polarizations caused a premature onset of the next reaction regime, or at very low current densities, when either spalling during charging or a reverse disproportionation reaction during discharging caused shifts in the plots of the ratios vs. current.

The determined ratios are consistent with a unit cell of 4 Ag's maintained throughout the oxidations, with the formation, first, of $Ag_2O \cdot Ag_2$, and, then, $Ag_2O \cdot Ag_2O_3$. For the reductions, it would appear that Ag is required to account for the 2/1 ratio, or else an intermediate Ag_4O_3 may be formed, as postulated by Watson, J. Chem. Soc. 89, 578(1906). Considering two 4 unit Ag cells, the changes in equivalent charges would be 2, 6, -3, and, then, -5.

Deviations from the determined ratios with porous electrodes may be anticipated if strong variations in current density develop along the electrode's thickness, or if the depth of penetration is altered during charge and discharge. For example, Q_1/Q_2 may appear to be less than 1/3 if the onset of AgO formation occurs prematurely because of poor reaction penetration during Ag_2O formation.

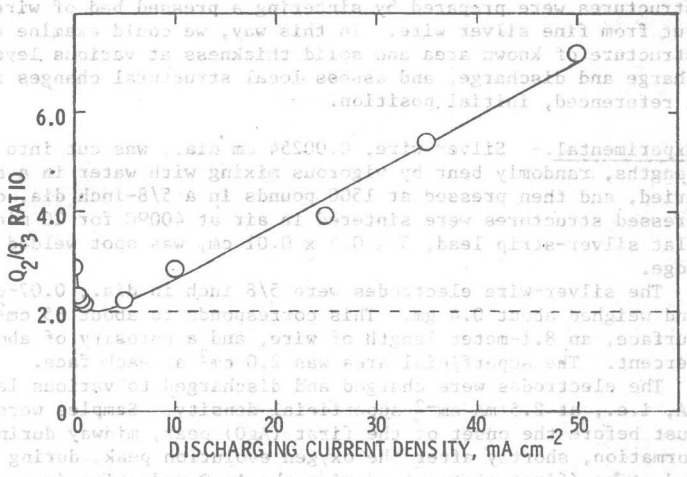

Fig. 1 Variation of the ratio, Q_2/Q_3, as the discharging current density is changed. A 2/1 ratio is approached as C.D. is decreased, until the AgO + Ag = Ag_2O reaction becomes competitive with the galvanostatic reduction. Charged at 0.7 mA cm^{-2}.

Abstract No. 3

OBSERVATIONS WITHIN A POROUS, SEGMENTED-WIRE SILVER OXIDE ELECTRODE

T. Katan and H. F. Bauman
Lockheed Palo Alto Research Laboratory
Palo Alto, California 94304

Typically, $Ag/Ag_2O/AgO$ electrodes are commercially prepared by electroforming porous silver structures. These structures consist of irregularly-shaped particles, bonded together by sintering. Examinations of the morphological changes within these electrodes can be made after charging and discharging to preselected levels, i.e., by optical microscopy and SEM analyses.

Such examinations, however, are difficult to interpret because the original shape of the silver is not uniform. Local variations in silver areas and thicknesses cause corresponding variations in local current densities, distributing reaction product irregularly.

In this study, we examined morphology in electrodes that were prepared from uniform, porous silver structures. The starting structures were prepared by sintering a pressed bed of wire segments, cut from fine silver wire. In this way, we could examine a porous structure of known area and solid thickness at various levels of charge and discharge, and assess local structural changes in terms of a referenced, initial position.

Experimental.- Silver wire, 0.00254 cm dia., was cut into 0.64-cm lengths, randomly bent by vigorous mixing with water in a blender, dried, and then pressed at 1500 pounds in a 5/8-inch dia. die. The pressed structures were sintered in air at 400°C for 20 min., and a flat silver-strip lead, 5 x 0.3 x 0.01 cm, was spot welded to the edge.

The silver-wire electrodes were 5/8 inch in dia., 0.07-cm thick, and weighed about 0.4 gm. This corresponds to about 65 cm^2 of wire surface, an 8.1-meter length of wire, and a porosity of about 70 percent. The superficial area was 2.0 cm^2 at each face.

The electrodes were charged and discharged to various levels at 10 mA, i.e., at 2.5 mA cm^{-2} superficial density. Samples were removed just before the onset of the first (AgO) peak, midway during AgO formation, shortly after the oxygen evolution peak, during AgO reduction (first plateau), during the Ag_2O reduction (second plateau), and after a complete reduction; this corresponded to 0.10, 0.15, 2.5, - 0.25, - 1.04, and - 1.93 A-min. of charge, respectively. After the treatments the electrodes were examined with optical microscopy and SEM.

Results and Discussion.- Morphological examinations made just before the onset of AgO formation revealed that only ca. 30 percent of the Ag surface was covered with obvious Ag_2O crystallites, about 0.7-micron across in size, the other Ag surface appearing smooth. This

suggests the occurrence of areas of relative passivity during the Ag_2O formation regime.

The AgO product, after onset of oxygen evolution, consisted of crystallites, mostly in the range of 0.3 to 3 microns across in size, forming a layer over all of the Ag surface, about 3 microns thick on the average. Although the film's surface appears to be granular with AgO crystallites, by the SEM examination, it also appears to be compact below the AgO/electrolyte surface, being more than 90-percent dense, by the examinations of cross sections with optical microscopy. The acquired charge of 1.93 A-min. at this time can be shown to correspond to a coverage of all the Ag surface with a 3.0-micron layer of AgO, from the known specific volume of AgO, in agreement with these microscopic observations.

During discharge at the AgO plateau, the larger AgO crystals on the AgO layer appear to be converted to smaller crystals, to about 0.3 micron in size, forming a layer resembling a spongy mass, with about 10-percent porosity, and still about 3-micron thick. At the Ag_2O plateau, the oxide layer appears to become somewhat thicker, about 5 micron, and more porous, about 15 percent. Cross sections indicated that AgO was reduced first at the top of the covering AgO layer, then in narrow regions penetrating to the substrate Ag, finally leaving isolated regions of relatively small amounts of AgO surrounded by Ag_2O, even in the Ag_2O-plateau regime.

Finally, after the complete reduction to Ag, the surface contained a layer of Ag nodules, about 1-micron across in size, with no clearly discernable crystal structure. It is estimated that these nodules increased the original surface area by threefold.

From the AgO film thickness, wire dia., and specific volumes of AgO and Ag, the largest Ag particle size that would be completely utilized under the conditions of the experiment is calculated to be 1 to 2-micron across in size. Particles larger than this would retain free silver at their core.

The Ag utilization in the wire electrode was only ca. 5 A-min. per gram of Ag because of the large wire dia., 25 micron, i.e., compare with 29.8 A-min. gm^{-1} for theoretical utilization. In related experiments, we normally obtained about 20 A-min. gm^{-1} utilization with similar electrodes prepared from commercially-available Ag powders having particles in the range of 0.2 to 3.5 micron.

Abstract No. 4

CURRENT DISTRIBUTION IN POROUS ZINC ELECTRODE. II. THE EFFECT OF ELECTROLYTE CONDUCTANCE

Ming-Biann Liu, B. R. Faulds*, G. M. Cook and N. P. Yao
Chemical Engineering Division
Argonne National Laboratory
9700 S. Cass Avenue
Argonne, Illinois 60439

The specific conductivity of 7.32 N KOH with various zincate concentrations (0 - 1.5 M) was measured. The result indicates that the specific conductivity of the electrolyte decreases linearly with increasing zincate concentration. A least-squares analysis of our data yields:

$$K = (0.637 \pm 0.011) - (0.159 \pm 0.009) C_{Zn(II)} \quad \text{mho/cm} \qquad (1)$$

or

$$\Lambda = (87 \pm 2) - (80 \pm 5) x_2 \quad \text{mho-cm}^{-1}\text{/equiv.} \qquad (2)$$

where K is the specific conductivity of the electrolyte, $C_{Zn(II)}$ is the molar zincate concentration, Λ is the equivalent conductance of the electrolyte and x_2 is the equivalent fraction of potassium zincate in the electrolyte. Equation (2) is a typical form which can be derived from a mixture rule.[1]

The specific conductivity data will be used to interprete the transient current distribution in a porous zinc electrode previously described.[2] The current distribution in the porous zinc electrode was highly nonuniform and the nonuniformity increased with time reaching a "steady state" level. A dimensionless group analysis[3] indicates that the behavior of the current distribution in the porous zinc electrode may arise when the electrolyte resistance is high in comparison to the charge-transfer resistance and mass transfer resistance of OH^- ions. In such a case, using a pseudo-steady state approximation, the current distribution at low current density may be expressed by the equation,[4,5]

$$\frac{i_m(y)}{I} = 1 - \frac{\sinh[\nu(1 - y)]}{\sinh(\nu)} \qquad (3)$$

where $i_m(y)$ is the integrated current density in the solid phase of the electrode, I is the overall current density of the electrode and y is the distance through the electrode normalized by the electrode thickness, L. Furthermore, in this equation,

$$\nu = L\sqrt{n\, a\, i_o\, F\, k_{eff}\, RT} \qquad (4)$$

where n is the number of electrons transferred in the electrode reaction, a is the specific surface area per unit volume, i_o is the exchange current density, k_{eff} is the effective conductivity in the pore electrolyte, F is Faraday's constant, R is the gas constant and T is the absolute temperature. By a least-squares procedure,[6] the best-fitted values of ν for the current distribution data are obtained. The current distribution data (represented by symbols) and the curves based on Eq. (3) with different values of ν are compared in Fig. 1. These values of ν increase with time and become constant at the "steady state". The increase of ν can be explained in terms of decrease in electrolyte conductance due to an increase in zincate concentration.

Acknowledgment

This work was financially supported by the U. S. Department of Energy, Division of Electrochemical Energy Systems and Office of Transportation programs. We thank Yardney Electric Company for providing nickel hydroxide electrodes.

References

1. D. G. Miller, Journal of Physical Chemistry, 71, 616 (1967).

2. Ming-Biann Liu, Y. Yamazaki, G. M. Cook and N. P. Yao, Extended Abstracts, The Electrochemical Society Fall Meeting, Hollywood, Florida, Vol. 80-2, p. 253 (1980).

3. Ming-Biann Liu, Y. Yamazaki, G. M. Cook and N. P. Yao, Transient Current Distributions in Porous Zinc Electrodes in KOH Electrolyte, ANL/OEPM-80-6, to be published.

4. J. Euler and W. Nonmacher, Electrochem. ACTA 2, 268 (1960).

5. J. Newman and C. W. Tobias, J. Electrochem. Soc. 109, 1183 (1962).

6. T. R. McCalla, Introduction to Numerical Methods and FORTRAN Programming, Johne Wiley & Sons, Inc. New York, NY 1967, p. 255.

*Participant in the 1980 summer graduate research participation program. Present address: Department of Chemistry, University of Wisconsin, Milwaukee.

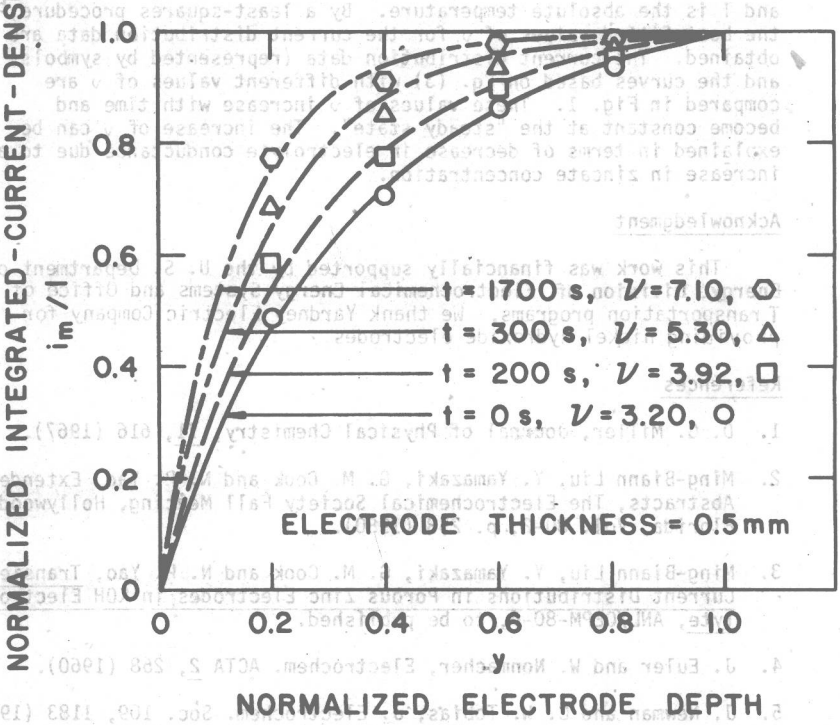

Fig. 1. Current Distributions in the Porous Zinc Electrode Discharged at 10 mA [Curves based on Eq. (3)]